Journal of Solid State Chemistry 182 (2009) 1206–1210

Contents lists available at ScienceDirect

Journal of Solid State Chemistry

journal homepage: www.elsevier.com/locate/jssc

Mesoscale assembly of NiO nanosheets into spheres

Meng Zhang *, Guojin Yan, Yonggai Hou, Chunhua Wang

School of Materials Science and Engineering, Henan University of Technology, Zhengzhou, Henan 450007, PR China

ARTICLE INFO

Article history:
Received 5 August 2008
Received in revised form
31 October 2008
Accepted 14 December 2008
Available online 8 January 2009

Keywords:
NiO
Mesoscale assembly
Tunable-surface areas
Electrochemical properties

ABSTRACT

NiO solid/hollow spheres with diameters about 100 nm have been successfully synthesized through thermal decomposition of nickel acetate in ethylene glycol at 200 °C. These spheres are composed of nanosheets about 3–5 nm thick. Introducing poly(vinyl pyrrolidone) (PVP) surfactant to reaction system can effectively control the products' morphology. By adjusting the quantity of PVP, we accomplish surface areas-tunable NiO assembled spheres from ~70 to ~200 $m^2 g^{-1}$. Electrochemical tests show that NiO hollow spheres deliver a large discharge capacity of 823 mA h g^{-1}. Furthermore, these hollow spheres also display a slow capacity-fading rate. A series of contrastive experiments demonstrate that the surface area of NiO assembled spheres has a noticeable influence on their discharge capacity.

1. Introduction

NiO has been extensively investigated as an important transition metal oxide. It finds a wide range of applications in various fields, such as catalysis [1,2], battery cathodes [3,4], gas sensors [5], electrochromic films [6], and fuel cell electrodes [7,8]. These applications are closely related to surface area of materials, wherefore, how to selective synthesizing NiO with different surface areas have not only fundamental scientific but also practical significance. In this paper, we present a facile technique for tuning the surface area of NiO by modifying the quantity of added poly(vinyl pyrrolidone) (PVP). And the discharge capacity of NiO was examined as an example of detecting the influence of products' surface area on their properties.

Recently, various chemical and physicochemical methods have been employed to produce nanosized NiO, including nanoparticles [9–11], nanorods [12,13], nanowires [14,15], nanosheets [16] and nanoplatelets [17]. However, mesoscale assembly of above nanosized building blocks to construct hierarchical structures remains a grand challenge [18–21]. Here we report a solvothermal route to assemble NiO nanosheets into spheres based on the geometric constraints among building blocks. In this process, ethylene glycol mainly acts as a high-boiling-point solvent [22], which can keep liquid state at a temperature sufficiently high to initiate and maintain the thermal decomposition of nickel acetate.

2. Experimental

Assembly of NiO nanosheets into hollow spheres was performed via a solvothermal approach. Details of a typical experiment are as follows: 1 mmol $Ni(CH_3COO)_2 \cdot 4H_2O$ and 0.3 g PVP (K-30) were added into a 50 ml Teflon-lined autoclave, which was filled with ethylene glycol (EG) up to 80% of the total volume. The autoclave was sealed and maintained at 200 °C for 24 h, and then was cool to room temperature naturally. The product was centrifuged and washed with distilled water and absolute ethanol several times, until black precipitate was collected. Finally, the obtained product was dried in vacuum at 60 °C for 4 h. Solid NiO spheres can be obtained when without PVP is added.

Powder X-ray diffraction (XRD) data were recorded by a Phillips X'Pert SUPER X-ray diffractometer with Cu $K\alpha$ radiation ($\lambda = 1.5418$ Å). The morphology and electron diffraction (ED) pattern were determined by a Hitachi 800 transmission electron microscope (TEM) and a field emission scanning electron microscope (EFSEM). The nanostructure of the as-prepared product was further characterized by a JEOL 2010 high-resolution transmission electron microscopy (HRTEM).

Electrochemical tests were conducted with Teflon cells. The positive electrodes were fabricated by pasting slurries of NiO powder (80 wt%), carbon black (10 wt%) and poly(vinylidene fluoride) (PVDF, 10 wt%) dissolved in N-methyl-pyrrolidinone (NMP) on Al foil strips by doctor blade technique. Then the strips were dried at 100 °C for 24 h in an air oven, pressed under 300 kg cm^{-2} pressure and kept at 100 °C for 48 h in a vacuum. Metallic lithium was used as negative electrode. The electrolyte was 1 M $LiPF_6$ in a 1:1 mixture of ethylene carbonate (EC)/diethyl carbonate (DEC); the separator was Celgard 2500. The cells were

* Corresponding author.
E-mail address: meng_zhang@haut.edu.cn (M. Zhang).

0022-4596/$ - see front matter © 2009 Published by Elsevier Inc.
doi:10.1016/j.jssc.2008.12.029

assembled in the glove box filled with highly pure argon gas. The cells were galvanostatically cycled in the 0.5–3.0 V range at a current density of 0.4 mA cm^{-2}.

3. Results and discussion

3.1. Characterization

The XRD patterns of the samples are shown in Fig. 1. Without PVP, the product exhibits the good crystallinity (Fig. 1a). The recorded diffraction peaks are well assigned to the cubic phase NiO structure (space group Fm_3/m; $a = 4.176$ Å; JCPDS 78-0643). Moreover, no other peak is observed belonging to the impurities, such as $Ni(CH_3COO)_2$ or Ni(OH)2, indicating the absolute transform from $Ni(CH_3COO)_2$ to NiO. In the XRD pattern of the sample prepared with 0.3 g PVP (Fig. 1b), the peaks intensity become weak, which reveals PVP makes against the crystallization of NiO.

Fig. 2a and b give the TEM images of NiO assembled spheres obtained in the absence of PVP. From Fig. 2a, one can see these assembled spheres are solid, and their average diameter is ca. 100 nm, showing a relatively narrow size distribution. The enlarged TEM image in Fig. 2b exhibits that individual solid spheres constitute of many interlaced nanosheets with the thickness < 5 nm. Correspondingly, NiO assembled spheres prepared with 0.3 g PVP reveal hollow nature (Fig. 2c–e), whose outer diameter is ca. 100 nm, and wall thickness is ca. 20 nm. The evidence for their hollow nature is the dark edges and pale centers of these spheres. An individual NiO hollow sphere is further displays in Fig. 2d, which shows sphere walls still consist of lots of nanosheets with an average thickness < 5 nm. Fig. 2e is the FESEM image of NiO hollow spheres where two features are apparent: high yield of products (above 90%) and the existence of broken spheres, which provides more convincing proof of their hollow nature.

The microstructure of NiO hollow spheres was confirmed by the HRTEM and SAED pattern. All hollow spheres combined by nanosheets are so firm that no unattached nanosheets were observed. Fig. 3a shows several nanosheets with the size of 20–60 nm and thickness of 3–5 nm (pointed by arrows). The SAED pattern of several nanosheets reveals the presence of polycrystalline loops (Fig. 3b), which correspond to (200) and (111) crystal

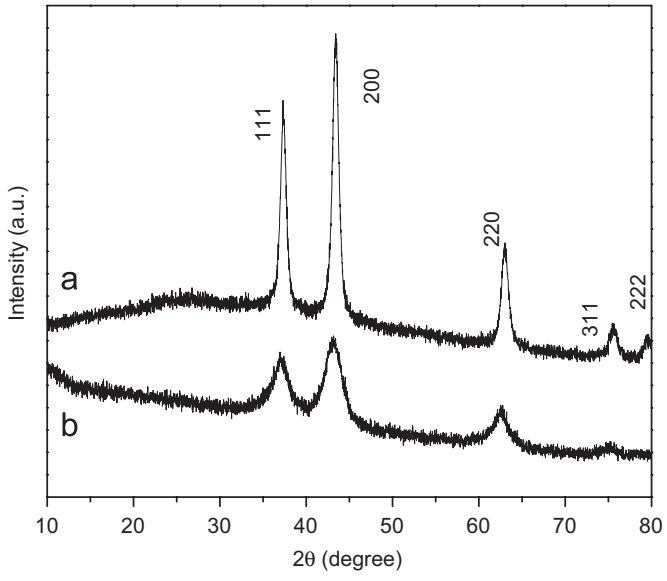

Fig. 1. XRD patterns of the samples prepared with 0 and 0.3 g PVP (from the top to bottom).

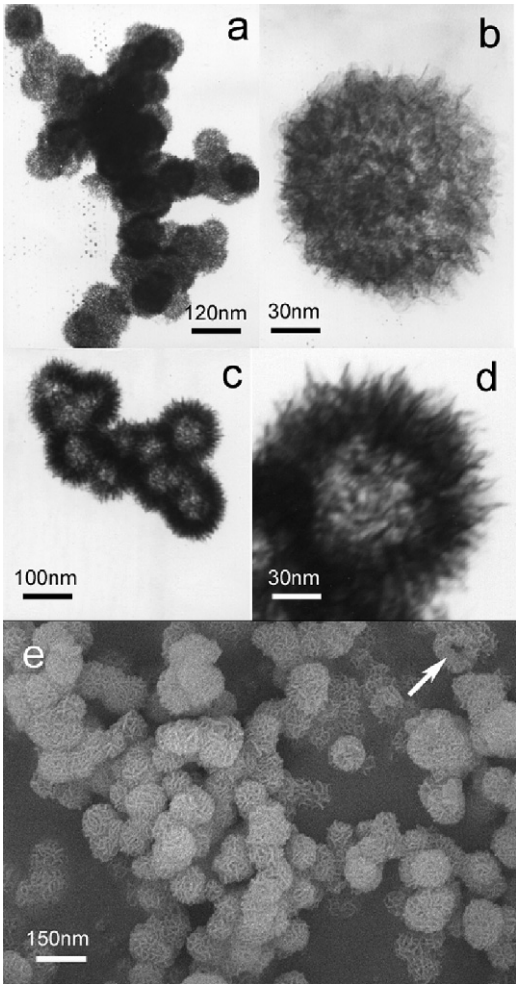

Fig. 2. TEM images of NiO solid spheres (a and b), TEM (c and d) and FESEM (e) images of NiO hollow spheres.

plans, respectively. The HRTEM image (Fig. 3c) taken from nanosheets shows the measured interplanar spacing is ca. 0.2 nm, which accords with the separation of {200} planes of cubic phase NiO.

3.2. Formation mechanism

By careful observing NiO spheres, we found interlaced nanosheets were not unorderly but oriented. These free-standing nanosheets are arrayed vertically to the spherical surface and point toward the spherical center (Fig. S1). This reveals the assembled spheres are primarily relies on the geometric constraints of NiO nanosheets, which present a distinct strategy to assemble building units into complex architectures [23–25]. As for the formation of hollow nature, we consider it should be attributed to a surfactant-assistant growth process. In this process, PVP molecules will congregate into spherical micelles, when their concentration is in an appropriate range. The outer surface of micelles is hydrophilic group (lactam), which is easily coated by $Ni(CH_3COO)_2$ due to the strong affinity of oxygen atoms for Ni^{2+} ions [26]. Under solvothermal conditions, $Ni(CH_3COO)_2$ decomposes into NiO on the interface. As the reaction proceeded, a shell constructed by NiO nanosheets deposit on the PVP micelles.

To further study the formation mechanism of NiO assembled spheres, we followed their growth steps and took notice of following facts: When the reaction was carried out without PVP,

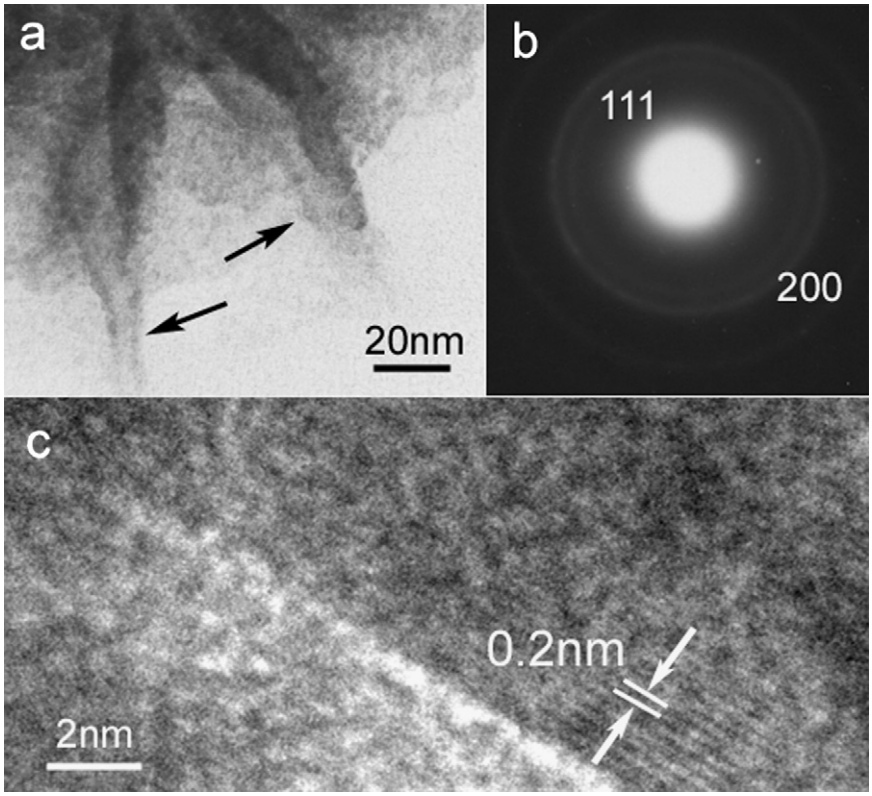

Fig. 3. TEM image (a), SAED pattern (b) and HRTEM image (c) of NiO nanosheets.

the products were mainly isolated NiO nanosheets after a short time, which gradually arranged together and formed solid spheres with the increasing time. When PVP existed in reaction system, NiO nanosheets firstly organized into loosely hollow spheres (Fig. S2), which developed in density with a longer time. Whether PVP exist or absent in reaction system, NiO nanosheets can assemble into spheres. That proves geometric constraints are indeed the drive forming assembled structure, since no other driving forces are used. The growth procedure of NiO hollow spheres indicates PVP plays a soft-template role for directing the formation of hollow morphology. It agrees with the before-mentioned surfactant-assistant growth mechanism.

It was tested via a series of experiments that some factors affect on the synthesis of NiO assembled spheres. The results are listed in Supporting Information (Table S1).

3.3. Tunable-surface areas

Fig. 4a shows N_2 adsorption/desorption isotherms of NiO spheres. The BET surface area (S_{BET}) of NiO solid spheres is 69.8 $m^2 g^{-1}$ (curve A), whereas that for NiO hollow spheres is as high as 201.8 $m^2 g^{-1}$ (curve B). The pore size distribution was calculated by BJH model [27] and shown in Fig. 4b. The pore size distributions of NiO solid spheres (curve A) are much broader than that of hollow spheres (curve B), whose mean diameter are 6.4 and 4.0 nm, respectively.

The difference of adsorption capability is great between the PVP-induced NiO hollows spheres and NiO solid spheres prepared without PVP. It implies that the samples' surface areas can be transformed in a wide range with varying the quantities of PVP.

Fig. 5 illustrates the effect of the quantity of PVP on the S_{BET}, and Dot A-G correspond to the NiO samples prepared with 0, 0.05, 0.1, 0.2, 0.3, 0.5 and 1.0 g PVP, respectively. Connecting these dots, one can obtain a fold line, which presents a general trend of S_{BET} with varying the amounts of PVP. The S_{BET} zoom when PVP is introduced into reaction system. Then, with adjusting the quantity of PVP from less to more the S_{BET} continuously rise. When 0.3 g PVP was added to the reaction system, the S_{BET} of samples would reach maximum; afterward, S_{BET} slightly lessens but still exceeds 190 $m^2 g^{-1}$ even if the quantity of PVP increased to 1 g. Especially, the S_{BET} is found to be linearly dependent on the quantity of PVP that ranged from 0.05 to 0.3 g. It is well known that the surface area are directly correlated to the porosity of porous materials, which may be changed by introducing surfactants [28]. Therefore, we deduce the accomplishment of tunable-surface areas comes from the pore-creating effects of PVP. That is, in the process to prepare NiO hollow spheres, PVP adsorb round NiO grains, and stuff up intercrystallite voids. After removing PVP, these voids emerge, and that enhances the volume of pores. The BJH cumulative desorption pore volumes of the NiO samples prepared with 0, 0.1 and 0.3 g PVP are 0.09, 0.13 and 0.16 $cm^3 g^{-1}$, respectively; theses data accord with our deduction. There exists a saturation limit of the PVP around 0.3 g. Above this limit, the excess PVP does not seem to be intercalated with NiO crystallites and shows little effect on the final pore structure [29]. Additionally, by analyzing the hysteresis loop of NiO hollow spheres, we forecast the pore's shape should be similar to bottle with narrow neck and vast cavity.

3.4. Electrochemical properties

Electrochemical performances of the as-prepared of NiO in the cell configuration NiO/Li have been evaluated. The charge/discharge process can be expressed as follows:

$$NiO + 2Li^+ + 2e^- \underset{\text{charge}}{\overset{\text{discharge}}{\rightleftharpoons}} Ni + Li_2O$$

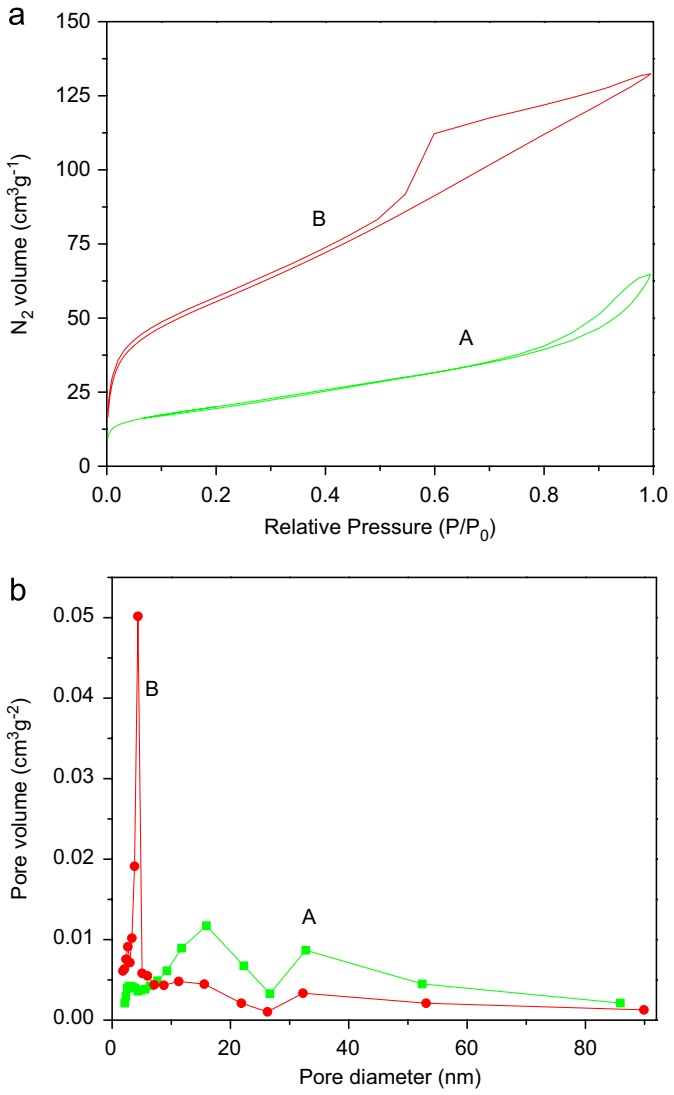

Fig. 4. (a) N_2 adsorption and desorption isotherms and (b) pore size distributions for NiO spheres (A: solid; B: hollow).

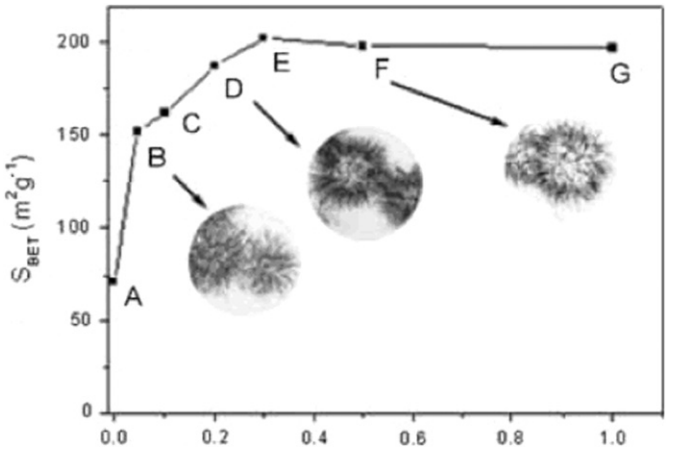

Fig. 5. Tuning S_{BET} by changing the quantity of PVP, the inset shows the typical morphology of corresponding samples.

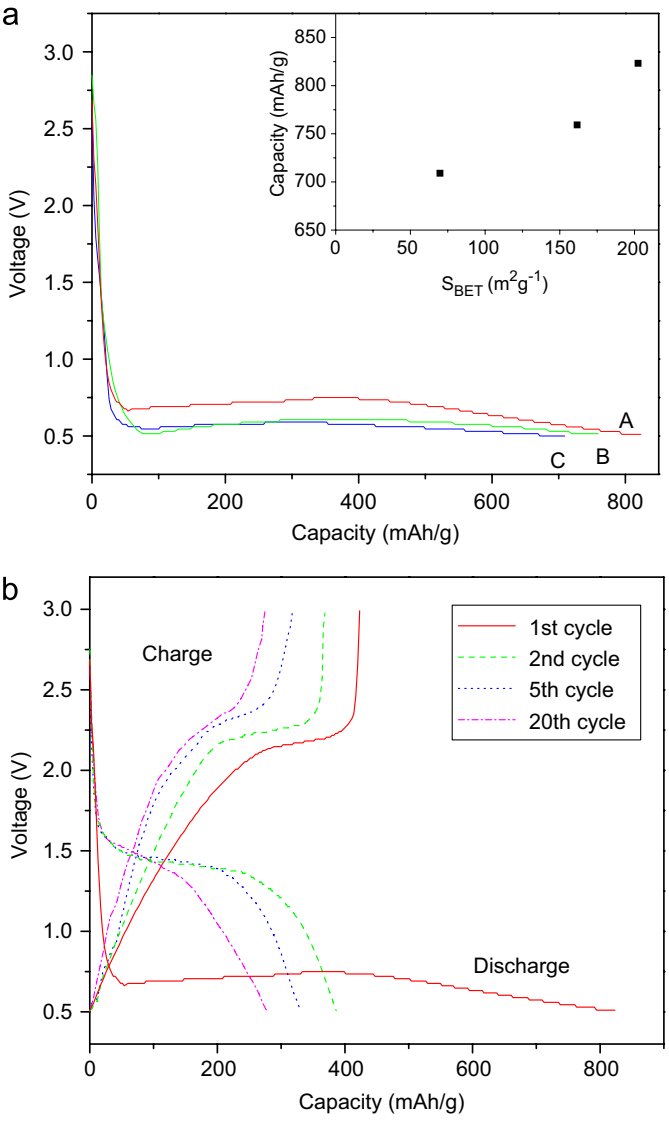

Fig. 6. (a) The first discharge curve of the NiO samples with different S_{BET}; the inset shows the discharge capacity becomes higher with the increased S_{BET} and (b) charge/discharge curves for NiO hollow spheres as electrode.

As shown in Fig. 6a, the first discharge capacity of sample A ($S_{BET} = 201.8\ m^2\ g^{-1}$) is around 823 mA h g^{-1}, which is higher than that of sample B ($S_{BET} = 161.1\ m^2\ g^{-1}$; 760 mA h g^{-1}) and C ($S_{BET} = 69.8\ m^2\ g^{-1}$; 709 mA h g^{-1}). All the NiO samples deliver quite high capacity, which is about twice that of the traditional graphite cathodes. It can be clearly observed that the discharge capacity becomes higher with the increased S_{BET} of NiO (inest in Fig. 6a), which is mainly attributed to several factors. First, the increased S_{BET} brings lots of interface structures and active sites, which facilitates the intercalation and deintercalation of Li^+ ions due to a shortening of the ion diffusion path in NiO electrode. Next, Li^+ ions can be freely intercalated not only in the NiO tunnels but also in the interface structures during the discharging process; that enhances the amount of intercalated Li^+ ions and improves the discharge capacity [30,31].

Fig. 6b displays the charge/discharge cycles of NiO hollow spheres at a current density of 0.4 mA cm^{-2}. After the initial cycle, there exists no substantial change in the following discharge curve shape; it remains similar to those in the second discharge. The second discharge capacity of NiO is 395 mA h g^{-1}. The large irreversible capacity maybe result from the decomposition of the electrolyte and subsequent formation of an organic layer deposited on the surface of particles that occur in the low-potential region for transition metal oxides [32]. The irreversible

capacity dramatically decreases at the second cycle, which suggest that a surface film can be formed effectively during the first cycle [33]. After 20 cycles, the specific capacity maintains about 300 mA h g^{-1}, so the NiO hollow spheres seem a promising anode materials for lithium-ion batteries in terms of slow capacity fading rate and high coulombic efficiency.

4. Conclusions

In summary, this paper describes a simple solvothermal method that leads to the mesoscale assembly of NiO nanosheets into spheres. The geometric constraints and surfactant-assistant growth mechanisms have been used to properly discuss assembly of NiO nanosheets. N_2 adsorption/desorption isotherms show the S_{BET} of NiO is tunable, which implies the feasibility to tune the surface areas of porous materials by adjusting the quantity of surfactant.

Acknowledgments

This work has been supported by Henan University of Technology (no. 2007BS057).

Appendix A. Supplementary material

Supplementary data associated with this article can be found in the online version at 10.1016/j.jssc.2008.12.029.

References

[1] D.S. Wang, R. Xu, X. Wang, Y.D. Li, Nanotechnology 17 (2006) 979.
[2] M.A. Gondal, M.N. Sayeed, Z. Seddigi, J. Hazard. Mater. 155 (2008) 83.
[3] P. Poizot, S. Laruelle, S. Grugeon, L. Dupont, J.M. Tarascon, Nature 407 (2000) 496.
[4] S.A. Needham, G.X. Wang, H.K. Liu, J. Power Sources 159 (2006) 254.
[5] I. Hotovy, V. Rehacek, P. Siciliano, S. Capone, L. Spiess, Thin Solid Films 418 (2002) 9.
[6] F. Li, H.Y. Chen, C.M. Wang, K.A. Hu, J. Electroanal. Chem. 531 (2002) 53.
[7] G.A. Niklasson, C.G. Granqvist, J. Mater. Chem. 17 (2007) 127.
[8] S.G. Kim, S.P. Yoon, J. Han, S.W. Nam, T.H. Lim, I.H. Oh, S.A. Hong, Electrochim. Acta 49 (2004) 3081.
[9] S.A. Makhlouf, F.T. Parker, F.E. Spada, A.E. Berkowitz, J. Appl. Phys. 81 (1997) 5561.
[10] M. Ghosh, K. Biswas, A. Sundaresan, C.N.R. Rao, J. Mater. Chem. 16 (2006) 106.
[11] T.L. Lai, Y.Y. Shu, G.L. Huang, C.C. Lee, C.B. Wang, J. Alloys Compd. 450 (2008) 318.
[12] K. Matsui, T. Kyotani, A. Tomita, Adv. Mater. 14 (2002) 1216.
[13] C.K. Xu, G.D. Xu, G.H. Wang, J. Mater. Sci. 38 (2003) 779.
[14] L.L. Wu, Y.S. Wu, H.Y. Wei, Y.C. Shi, C.X. Hu, Mater. Lett. 58 (2004) 2700.
[15] C. Xu, K. Hong, S. Liu, G. Wang, X. Zhao, J. Cryst. Growth 255 (2003) 308.
[16] Z.H. Liang, Y.J. Zhu, X.L. Hu, J. Phys. Chem. B 108 (2004) 3488.
[17] X. Wang, L. Li, Y.G. Zhang, S.T. Wang, Z.D. Zhang, L.F. Fei, Y.T. Qian, Cryst. Growth Des. 6 (2006) 2163.
[18] D.B. Wang, C.X. Song, Z.S. Hu, X. Fu, J. Phys. Chem. B 109 (2005) 1125.
[19] Y. Wang, Q.S. Zhu, H.G. Zhang, Chem. Commun. (2005) 5231.
[20] X.M. Ni, Y.F. Zhang, D.Y. Tian, H.G. Zheng, X.W. Wang, J. Cryst. Growth 306 (2007) 418.
[21] C.S. Shi, G.Q. Wang, N.Q. Zhao, X.W. Du, J.J. Li, Chem. Phys. Lett. 454 (2008) 75.
[22] Y.L. Wang, X.C. Jiang, T. Herricks, Y.N. Xia, J. Phys. Chem. B 108 (2004) 8631.
[23] Y.L. Hou, H. Kondoh, T. Ohta, Chem. Mater. 17 (2005) 3994.
[24] G.Z. Shen, Y. Bando, J.Q. Hu, D. Golberg, Appl. Phys. Lett. 90 (2007) 123101.
[25] H.C. Zeng, Int. J. Nanotechnol. 4 (2007) 329.
[26] J.C. Bao, Y.Y. Liang, Z. Xu, L. Si, Adv. Mater. 15 (2003) 1832.
[27] E.P. Barrett, L.G. Joyner, P.H. Halenda, J. Am. Chem. Soc. 73 (1951) 373.
[28] Z. Shen, G.Z. Zhao, G.T. Wang, Colloid and Surface Chemistry, Chemical Industry Press, Beijing, 2004.
[29] H.Y. Zhu, J.D. Richesv, J.C. Barry, Chem. Mater. 14 (2002) 2086.
[30] E. Machefaux, A. Verbaere, D. Guyomard, Ionics 11 (2005) 24.
[31] Y.J. Yang, C.D. Huang, Chem. Ind. Eng. Prog. 25 (2006) 383.
[32] D. Larcher, C. Masquelier, D. Bonnin, Y. Chabre, V. Masson, J.B. Leriche, J.M. Tarascon, J. Electrochem. Soc. 150 (2003) A133.
[33] D. Takayuki, F. Akihito, I. Yasutoshi, A. Takeshi, O. Zempachi, N. Kiyoharu, A. Toshihiro, Electrochem. Commun. 7 (2005) 10.